

A Study of Charmless Hadronic B Decays to $h\pi^0$ Final States

The Belle Collaboration

Abstract

We report preliminary results on a study of $B \rightarrow h\pi^0$ decays using a 5.3 fb^{-1} data sample collected at the $\Upsilon(4S)$ resonance with the Belle detector at the KEKB e^+e^- storage ring. Clear signatures for $B^+ \rightarrow K^+\pi^0$ and $B^0 \rightarrow K^0\pi^0$ have been seen and the corresponding branching ratios are measured to be $(1.88_{-0.49}^{+0.55} \pm 0.23) \times 10^{-5}$ and $(2.10_{-0.78-0.23}^{+0.93+0.25}) \times 10^{-5}$, respectively. No statistically significant signal is observed for $B^+ \rightarrow \pi^+\pi^0$ and we report a 90% CL. upper limit of 1.01×10^{-5} .

Typeset using REVTeX

A. Abashian⁴⁴, K. Abe⁸, K. Abe³⁶, I. Adachi⁸, Byoung Sup Ahn¹⁴, H. Aihara³⁷,
 M. Akatsu¹⁹, G. Alimonti⁷, K. Aoki⁸, K. Asai²⁰, M. Asai⁹, Y. Asano⁴², T. Aso⁴¹,
 V. Aulchenko², T. Aushev¹², A. M. Bakich³³, E. Banas¹⁵, S. Behari⁸, P. K. Behera⁴³,
 D. Beilene², A. Bondar², A. Bozek¹⁵, T. E. Browder⁷, B. C. K. Casey⁷, P. Chang²³,
 Y. Chao²³, B. G. Cheon³², S.-K. Choi⁶, Y. Choi³², Y. Doi⁸, J. Dragic¹⁷, A. Drutskoy¹²,
 S. Eidelman², Y. Enari¹⁹, R. Enomoto^{8,10}, C. W. Everton¹⁷, F. Fang⁷, H. Fujii⁸,
 K. Fujimoto¹⁹, Y. Fujita⁸, C. Fukunaga³⁹, M. Fukushima¹⁰, A. Garmash^{2,8}, A. Gordon¹⁷,
 K. Gotow⁴⁴, H. Guler⁷, R. Guo²¹, J. Haba⁸, T. Haji⁴, H. Hamasaki⁸, K. Hanagaki²⁹,
 F. Handa³⁶, K. Hara²⁷, T. Hara²⁷, T. Haruyama⁸, N. C. Hastings¹⁷, K. Hayashi⁸,
 H. Hayashii²⁰, M. Hazumi²⁷, E. M. Heenan¹⁷, Y. Higashi⁸, Y. Higasino¹⁹, I. Higuchi³⁶,
 T. Higuchi³⁷, T. Hirai³⁸, H. Hirano⁴⁰, M. Hirose¹⁹, T. Hojo²⁷, Y. Hoshi³⁵, K. Hoshina⁴⁰,
 W.-S. Hou²³, S.-C. Hsu²³, H.-C. Huang²³, Y.-C. Huang²¹, S. Ichizawa³⁸, Y. Igarashi⁸,
 T. Iijima⁸, H. Ikeda⁸, K. Ikeda²⁰, K. Inami¹⁹, Y. Inoue²⁶, A. Ishikawa¹⁹, R. Itoh⁸,
 G. Iwai²⁵, M. Iwai⁸, H. Iwasaki⁸, Y. Iwasaki⁸, D. J. Jackson²⁷, P. Jalocha¹⁵, H. K. Jang³¹,
 M. Jones⁷, R. Kagan¹², H. Kakuno³⁸, J. Kaneko³⁸, J. H. Kang⁴⁵, J. S. Kang¹⁴,
 P. Kapusta¹⁵, K. Kasami⁸, N. Katayama⁸, H. Kawai³, M. Kawai⁸, N. Kawamura¹,
 T. Kawasaki²⁵, H. Kichimi⁸, D. W. Kim³², Heejong Kim⁴⁵, H. J. Kim⁴⁵, Hyunwoo Kim¹⁴,
 S. K. Kim³¹, K. Kinoshita⁵, S. Kobayashi³⁰, S. Koike⁸, Y. Kondo⁸, H. Konishi⁴⁰,
 K. Korotushenko²⁹, P. Krokovny², R. Kulasiri⁵, S. Kumar²⁸, T. Kuniya³⁰, E. Kurihara³,
 A. Kuzmin², Y.-J. Kwon⁴⁵, M. H. Lee⁸, S. H. Lee³¹, C. Leonidopoulos²⁹, H.-B. Li¹¹,
 R.-S. Lu²³, Y. Makida⁸, A. Manabe⁸, D. Marlow²⁹, T. Matsubara³⁷, T. Matsuda⁸,
 S. Matsui¹⁹, S. Matsumoto⁴, T. Matsumoto¹⁹, K. Misono¹⁹, K. Miyabayashi²⁰,
 H. Miyake²⁷, H. Miyata²⁵, L. C. Moffitt¹⁷, G. R. Moloney¹⁷, G. F. Moorhead¹⁷,
 N. Morgan⁴⁴, S. Mori⁴², T. Mori⁴, A. Murakami³⁰, T. Nagamine³⁶, Y. Nagasaka¹⁸,
 Y. Nagashima²⁷, T. Nakadaira³⁷, T. Nakamura³⁸, E. Nakano²⁶, M. Nakao⁸, H. Nakazawa⁴,
 J. W. Nam³², S. Narita³⁶, Z. Natkaniec¹⁵, K. Neichi³⁵, S. Nishida¹⁶, O. Nitoh⁴⁰,
 S. Noguchi²⁰, T. Nozaki⁸, S. Ogawa³⁴, R. Ohkubo⁸, T. Ohshima¹⁹, Y. Ohshima³⁸,
 T. Okabe¹⁹, T. Okazaki²⁰, S. Okuno¹³, S. L. Olsen⁷, W. Ostrowicz¹⁵, H. Ozaki⁸,
 P. Pakhlov¹², H. Palka¹⁵, C. S. Park³¹, C. W. Park¹⁴, H. Park¹⁴, L. S. Peak³³, M. Peters⁷,
 L. E. Piiilonen⁴⁴, E. Prebys²⁹, J. Raaf⁵, J. L. Rodriguez⁷, N. Root², M. Rozanska¹⁵,
 K. Rybicki¹⁵, J. Ryuko²⁷, H. Sagawa⁸, Y. Sakai⁸, H. Sakamoto¹⁶, H. Sakaue²⁶,
 M. Satapathy⁴³, N. Sato⁸, A. Satpathy^{8,5}, S. Schrenk⁴⁴, S. Semenov¹², Y. Settai⁴,
 M. E. Sevier¹⁷, H. Shibuya³⁴, B. Shwartz², A. Sidorov², V. Sidorov², S. Stanić⁴², A. Sugi¹⁹,
 A. Sugiyama¹⁹, K. Sumisawa²⁷, T. Sumiyoshi⁸, J. Suzuki⁸, J.-I. Suzuki⁸, K. Suzuki³,
 S. Suzuki¹⁹, S. Y. Suzuki⁸, S. K. Swain⁷, H. Tajima³⁷, T. Takahashi²⁶, F. Takasaki⁸,
 M. Takita²⁷, K. Tamai⁸, N. Tamura²⁵, J. Tanaka³⁷, M. Tanaka⁸, Y. Tanaka¹⁸,
 G. N. Taylor¹⁷, Y. Teramoto²⁶, M. Tomoto¹⁹, T. Tomura³⁷, S. N. Tovey¹⁷, K. Trabelsi⁷,
 T. Tsuboyama⁸, Y. Tsujita⁴², T. Tsukamoto⁸, T. Tsukamoto³⁰, S. Uehara⁸, K. Ueno²³,
 N. Ujiie⁸, Y. Unno³, S. Uno⁸, Y. Ushiroda¹⁶, Y. Usov², S. E. Vahsen²⁹, G. Varner⁷,
 K. E. Varvell³³, C. C. Wang²³, C. H. Wang²², M.-Z. Wang²³, T.-J. Wang¹¹, Y. Watanabe³⁸,
 E. Won³¹, B. D. Yabsley⁸, Y. Yamada⁸, M. Yamaga³⁶, A. Yamaguchi³⁶, H. Yamaguchi⁸,
 H. Yamamoto⁷, H. Yamaoka⁸, Y. Yamaoka⁸, Y. Yamashita²⁴, M. Yamauchi⁸, S. Yanaka³⁸,
 M. Yokoyama³⁷, K. Yoshida¹⁹, Y. Yusa³⁶, H. Yuta¹, C.-C. Zhang¹¹, H. W. Zhao⁸,
 Y. Zheng⁷, V. Zhilich², and D. Žontar⁴²

¹Aomori University, Aomori

- ²Budker Institute of Nuclear Physics, Novosibirsk
- ³Chiba University, Chiba
- ⁴Chuo University, Tokyo
- ⁵University of Cincinnati, Cincinnati, OH
- ⁶Gyeongsang National University, Chinju
- ⁷University of Hawaii, Honolulu HI
- ⁸High Energy Accelerator Research Organization (KEK), Tsukuba
- ⁹Hiroshima Institute of Technology, Hiroshima
- ¹⁰Institute for Cosmic Ray Research, University of Tokyo, Tokyo
- ¹¹Institute of High Energy Physics, Chinese Academy of Sciences, Beijing
- ¹²Institute for Theoretical and Experimental Physics, Moscow
- ¹³Kanagawa University, Yokohama
- ¹⁴Korea University, Seoul
- ¹⁵H. Niewodniczanski Institute of Nuclear Physics, Krakow
- ¹⁶Kyoto University, Kyoto
- ¹⁷University of Melbourne, Victoria
- ¹⁸Nagasaki Institute of Applied Science, Nagasaki
- ¹⁹Nagoya University, Nagoya
- ²⁰Nara Women's University, Nara
- ²¹National Kaohsiung Normal University, Kaohsiung
- ²²National Lien-Ho Institute of Technology, Miao Li
- ²³National Taiwan University, Taipei
- ²⁴Nihon Dental College, Niigata
- ²⁵Niigata University, Niigata
- ²⁶Osaka City University, Osaka
- ²⁷Osaka University, Osaka
- ²⁸Panjab University, Chandigarh
- ²⁹Princeton University, Princeton NJ
- ³⁰Saga University, Saga
- ³¹Seoul National University, Seoul
- ³²Sungkyunkwan University, Suwon
- ³³University of Sydney, Sydney NSW
- ³⁴Toho University, Funabashi
- ³⁵Tohoku Gakuin University, Tagajo
- ³⁶Tohoku University, Sendai
- ³⁷University of Tokyo, Tokyo
- ³⁸Tokyo Institute of Technology, Tokyo
- ³⁹Tokyo Metropolitan University, Tokyo
- ⁴⁰Tokyo University of Agriculture and Technology, Tokyo
- ⁴¹Toyama National College of Maritime Technology, Toyama
- ⁴²University of Tsukuba, Tsukuba
- ⁴³Utkal University, Bhubaneswer
- ⁴⁴Virginia Polytechnic Institute and State University, Blacksburg VA
- ⁴⁵Yonsei University, Seoul

I. INTRODUCTION

Charmless hadronic B decays can be described by external and internal W emission, gluonic and electromagnetic penguins, W exchange and annihilation diagrams. Measurements of the branching fractions of various charmless B decays probe the CKM [1] sector of the standard model [2]. It has been suggested that an isospin analysis can be performed [3] to extract the second CP violation angle $\phi_2(/\alpha)$ using the decay rates of $B^+ \rightarrow K^+\pi^0$, $B^+ \rightarrow K^0\pi^+$ and $B^0 \rightarrow K^+\pi^-$, along with the rates and the CP asymmetry in $B^0 \rightarrow K_S\pi^0$. The third CP violation angle $\phi_3(/\gamma)$ may be also determinable via the $\pi\pi$ and $K\pi$ branching ratios [4].

Recent CLEO results based on 9.7 fb^{-1} of integrated luminosity at $\Upsilon(4S)$ CM energies indicate that the branching ratios are $(1 \sim 2) \times 10^{-5}$ for the $K\pi$ modes and $(3 \sim 7) \times 10^{-6}$ for the $\pi^+\pi$ modes. With more than 5 fb^{-1} data collected in Belle, we perform a $B \rightarrow h\pi^0$ search to check CLEO results and prepare for a future direct CP asymmetry search. In this paper, h stands for K^+ , π^+ , or K_S .

We analyzed 5.3 fb^{-1} of data which corresponds to $5.5 \times 10^6 B\bar{B}$ events. This data sample was collected by the Belle detector [5] on the $\Upsilon(4S)$ resonance at the KEKB asymmetric e^+e^- storage ring [6]. The beam energy is 3.5 GeV for positrons and 8.0 GeV for electrons. The Belle detector is described in [5] and we only briefly describe the apparatus used in this analysis. Charged particle tracking is provided by three layers of double-sided silicon vertex detector (SVD) [7] and a cylindrical drift chamber (CDC) [8], which consists of 50 layers segmented into 5 axial and 4 stereo superlayers. Charged tracks are reconstructed inside a 1.5 T solenoidal magnet using the incremental Kalman filtering technique to successively update the track parameters after associating CDC and SVD hits in each layer. The charged particle acceptance covers the angle between $\theta = 17^\circ$ and 150° in the laboratory frame. Charged hadrons are identified from three subsystems: dE/dx information from the CDC, a mosaic of 1188 aerogel Čerenkov counters (ACC) [9] covering the range $1 < P_{lab} < 4 \text{ GeV}/c$, and a time-of-flight scintillation counter system (TOF) [10] with 100 ps time resolution ($P_{lab} < 1.5 \text{ GeV}/c$). Outside the tracking and particle identification systems is an electromagnetic calorimeter (ECL), which consists of 8736 CsI crystals with $16.2 X_0$ depth [11].

II. DATA ANALYSIS

In the $h\pi^0$ search, π^0 s are identified by combining two photon clusters and requiring their combined mass be within $16.2 \text{ MeV}/c^2$ of the nominal π^0 mass. For each π^0 candidate we then perform a π^0 mass constraint using the error matrix for each photon cluster. Hadron identification is provided by the ACC and CDC. Since the charged hadrons in the $h^+\pi^0$ channel have momenta above $1.5 \text{ GeV}/c$, TOF information is not used. We combine the K/π probability from the ACC and dE/dx to form a K/π likelihood $L(K)/L(\pi)$. K/π separation is then achieved by cutting on the likelihood ratio, $L_K/(L_\pi + L_K)$. Charged tracks with likelihood ratio greater than 0.6 are identified as kaons and less than 0.4 as pions. K_S candidates are formed by vertex constraining two oppositely charged particles and selecting candidates with vertex fit $\chi^2 < 10$ and masses within 3.5 sigma of the nominal K_S mass. In addition, we require that the transverse distance between the K_S vertex and the run average beam position is greater than 0.2 cm.

The $h\pi^0$ candidates are identified using two variables: the beam constrained mass M_b and the energy difference ΔE in the e^+e^- center of mass frame. The definitions of M_b and ΔE are

$$M_b = \sqrt{E_{\text{beam}}^2 - (\vec{P}_h + \vec{P}_{\pi^0})^2}, \quad (1)$$

$$\Delta E = E_{h\pi^0} - E_{\text{beam}}. \quad (2)$$

$$(3)$$

We select events with the criteria $M_b > 5.2 \text{ GeV}/c^2$ and $-0.45 \text{ GeV} < \Delta E < 0.15 \text{ GeV}$ and define the region with $M_b > 5.27 \text{ GeV}/c^2$ and $-0.15 \text{ GeV} < \Delta E < 0.05 \text{ GeV}$ as the signal region and $M_b < 5.26 \text{ GeV}/c^2$ as the sideband region. After the M_b and ΔE selections, 9393, 19788, and 1255 events are found for $K^+\pi^0$, $\pi^+\pi^0$, and $K_S\pi^0$ modes, respectively.

To further distinguish signals from background, we rely on shape variables to discriminate between $B\bar{B}$ events and jet-like events from the $e^+e^- \rightarrow q\bar{q}$ continuum. Generic $B\bar{B}$ background is negligible. The shape variable $\cos\theta_B$ is defined as the cosine of the angle between the B flight direction and the beam axis. Since the helicity of $\Upsilon(4S)$ produced from e^+e^- collisions is ± 1 , we expect a $\sin^2\theta_B$ distribution for the B flight direction. The variable $\cos\theta_{\text{thrust}}$ is the cosine of the angle between the π^0 direction and the thrust axis of the remaining particles of the event after removing the B daughters, h and π^0 . Another variable used in this analysis is *Sphericity*, which is defined as the scalar sum of the transverse momenta of all particles outside a 45° cone around the π^0 direction divided by their total momentum sum. We also use a set of variables extended from the Fox-Wolfram moments [12], which are defined as:

$$R_l = \frac{H_l}{H_0}, \quad (4)$$

$$H_l = \sum_{ij} |\vec{p}_i| |\vec{p}_j| P_l(\cos\theta_{ij}), \quad (5)$$

where l is the l th moment, \vec{p}_i is the momentum of the i th particle in an event, and $P_l(\cos\theta_{ij})$ is the l th Legendre polynomial. In our new definition, we separate the original Fox-Wolfram moment into three parts:

$$R_l = R_l^{ss} + R_l^{so} + R_l^{oo}, \quad (6)$$

where, *ss* stands for particles i and j both coming from B daughters, *so* means that one particle is from a B daughter and the other is from the remaining particles in the event. and *oo* indicates that both particles are not the B daughters. These new variables are named super Fox-Wolfram moments (SFW). Since R_l^{ss} is strongly correlated with other variables (M_b and $\cos\theta_B$), we do not include it. Further studies show that R_1^{so} , R_3^{so} and R_1^{oo} are correlated with the beam constrained mass M_b ; therefore we also remove these three variables. In this analysis we combine SFW variables up to $l = 4$ into our shape variables. Since five of the SFW variables, $\cos\theta_{\text{thrust}}$, and *Sphericity* are not totally independent, we combine these seven variables into a Fisher discriminant,

$$\mathcal{F} = \vec{\alpha} \cdot \vec{R}, \quad (7)$$

where \vec{R} is the vector of the seven shape variables and $\vec{\alpha}$ is the weight vector determined by optimizing the separation between signal events and continuum background. Note that this Fisher variable is the one that describes the event topology.

After forming the shape variable Fisher discriminant, we end up with four variables in our analyses: M_b , ΔE , $\cos\theta_B$, and the Fisher discriminant. To further reduce the background fraction of our data sample, we require that the $|\cos\theta_{\text{thrust}}| < 0.8$ for both the $K^+\pi^0$ and $K_S\pi^0$ samples.

TABLE I. Function forms of various PDFs

	Signal	Background
M_b	Crystal Ball Line	ARGUS function
ΔE	Crystal Ball Line	Straight line
$\cos \theta_B$	2nd order Legendre Pol.	Straight line
Fisher	Double Bifurcated Gaussian	Double Bifurcated Gaussian

Since the $\pi^+\pi^0$ mode has a larger background and the expected signal yield is small, we apply a tighter constraint, $|\cos \theta_{\text{thrust}}| < 0.6$. The corresponding number of events after the $\cos \theta_{\text{thrust}}$ cut are 2198, 1436, and 335 for $K^+\pi^0$, $\pi^+\pi^0$ and $K_S\pi^0$ channels, respectively.

We perform a Maximum Likelihood (ML) fit to obtain signal yield, using the standard fitting package MINUIT. The likelihood function is defined as

$$L(f_s) = \prod_i [f_s P_S(X_i) + (1 - f_s) P_B(X_i)], \quad (8)$$

where f_s is the fraction of the signal yield, P_S is the product of all the signal probability densities of the four input variables, P_B is the background probability density, and i is the i th event. The signal and background probability functions (PDF) are obtained using Monte Carlo signal events and data events in the sideband area. Figure 1 shows the distributions of those four variables. The solid histograms are signal MC events and the points with error bars are data in the sideband region. Superimposed on those histograms are the PDFs used in the likelihood fit. The exact functional forms of various PDFs are given in Table I.

Since we expect quite a sizeable $K^+\pi^0$ feed down in the $\pi^+\pi^0$ sample, an extra term f_{sk} is included in the likelihood. This component has a signal shape but is shifted in ΔE by -40 MeV and its normalization is determined from the size of the observed $B^+ \rightarrow K^+\pi^0$ signal, the kaon identification efficiency, the K to π fake rate, and the efficiency of the $\cos \theta_{\text{thrust}}$ cut.

We then use the events in the π^0 sideband region and K_S sideband region (4-6 σ away from their nominal masses) to test our fitter. No signal events are found in the sideband sample, indicating the stability of our likelihood method. To further check the reliability of our fit results, we apply the likelihood ratio analysis to compare the obtained yields. The likelihood ratio (LR) is defined as:

$$LR = \frac{L_s}{L_s + L_b}, \quad (9)$$

where L_s/L_b is the signal/background likelihood obtained using the variables $\cos \theta_B$ and the Fisher discriminant. We then perform a fit to the M_b and ΔE distributions after applying the criteria, $|\cos \theta_{\text{thrust}}| < 0.9$ and $LR > 0.8$ for the $K^+\pi^0$ and $K_S\pi^0$ modes. We apply a tighter constraint $LR > 0.9$ for the $\pi^+\pi^0$ mode due to the poorer signal to background ratio. The obtained yields are compared with the ML fit results after taking into account their corresponding efficiencies. Both methods give consistent results while the ML fit has a factor of two better efficiency.

III. RESULTS

The results of the ML fit are given in Table II. The first error in column 3 is the statistical error while the second one is the systematic error from the fit. The systematic error of the fit is estimated

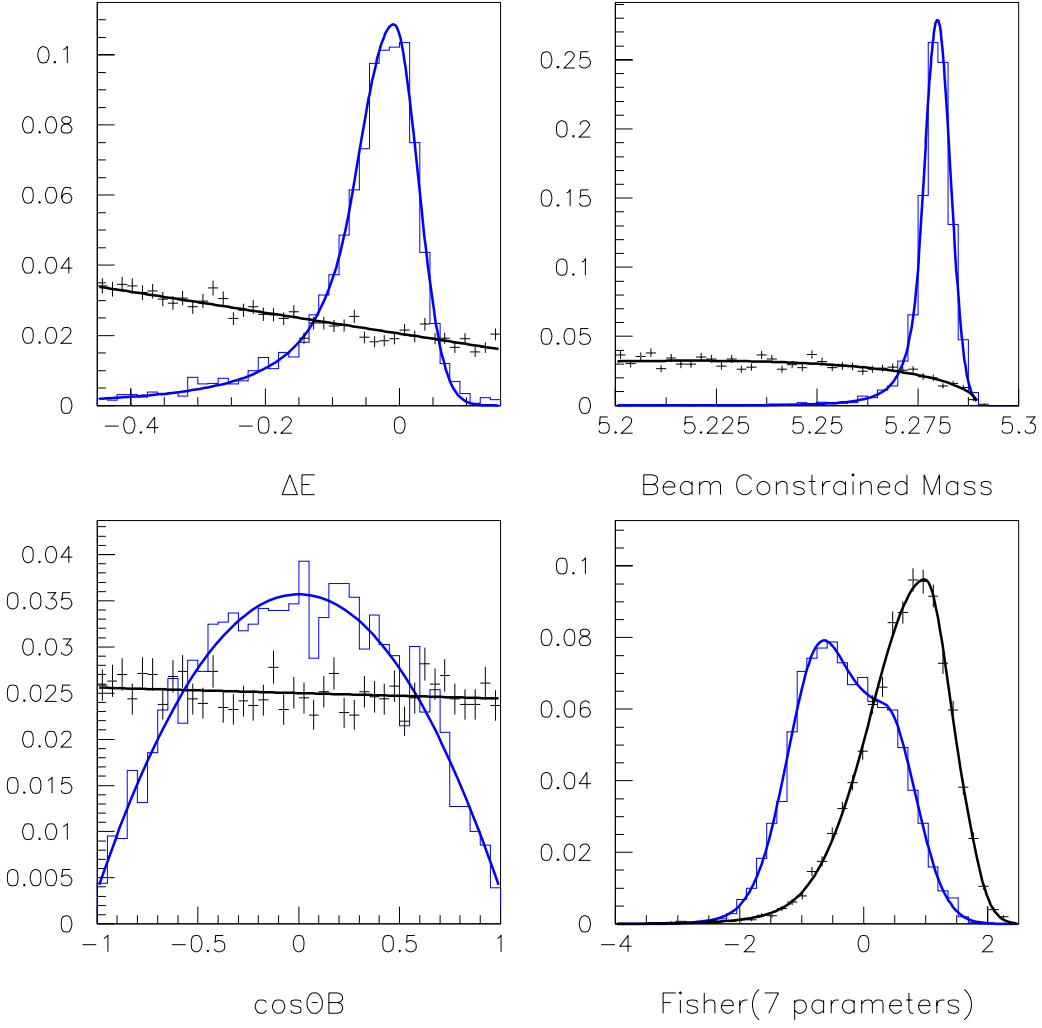


FIG. 1. The distributions of M_b , ΔE , $\cos\theta_B$, and the Fisher discriminant for signal MC events and the data in the sideband region. Solid histograms are signal MC; points with error bars are sideband data. Superimposed on the histograms are the PDFs used in the likelihood fit.

TABLE II. The ML fit results in $h\pi^0$ search.

Mode	N_{tot}	Yield	Significance	Efficiency
$K^+\pi^0$	2198	$32.3^{+9.4+2.4}_{-8.4-2.2}$	5.0σ	31.3%
$\pi^+\pi^0$	1486	$5.4^{+5.7+1.0}_{-4.4-1.1}$	1.3σ	29.9%
$K^0\pi^0$	335	$10.8^{+4.8+0.7}_{-4.0-0.5}$	3.9σ	18.7 %

by quadratically summing all the deviations of the signal yield after varying each parameter of the PDFs by one sigma at a time. Figure 2 displays the dependence of $-2\ln(\mathcal{L}/\mathcal{L}_{\max})$ on the number of signal events. The corresponding statistical significances of the deviations from 0 are 5.0σ , 1.3σ , and 3.9σ for the $K^+\pi^0$, $\pi^+\pi^0$, and $K_S\pi^0$ modes, respectively. The M_b and ΔE projection plots are shown in Fig. 3.

The π^0 reconstruction efficiency is checked by studying $D^0 \rightarrow K^-\pi^+\pi^0$ and $D^0 \rightarrow K^-\pi^+$ decays. We compare the ratio of the number of events between these two modes in data with Monte Carlo prediction. In this study π^0 s are required to be high momentum ($P > 1.5$ GeV/c) and all tracks with $P > 0.5$ GeV/c. The systematic error on the π^0 reconstruction efficiency estimated in this ratio method is around 7%. The charged track reconstruction efficiency is calibrated within 1.7% uncertainty using inclusive high momentum $\eta \rightarrow \pi^+\pi^-\pi^0$ and $\eta \rightarrow \gamma\gamma$ while requiring the $\pi^+\pi^-$ be in the same momentum range as the B daughters. The reconstruction efficiency for $K^0 \rightarrow \pi^+\pi^-$ is tested using K^0 candidates in the B sideband area. We study the inefficiency by switching on and off the χ^2 and flight distance cuts and then comparing the result with the Monte Carlo expectation. A 7% uncertainty in the K_S efficiency is obtained. The efficiency and fake rate of our particle identification procedures are studied using the continuum $D^{*+} \rightarrow D^0\pi^+$ sample. The identification efficiency and the $K^+ \rightarrow \pi^+$ fake rate for high momentum kaons are 78% and 18%, respectively; the corresponding values for pions are 90% and 7%. The final reconstruction efficiencies for $h\pi^0$ events are given in Table II with 10% systematic uncertainty. The number of $K^+\pi^0$ to $\pi^+\pi^0$ feed down is estimated to be $5.4^{+1.6}_{-1.4}$.

The final branching fractions of for $h\pi^0$ are:

$$\begin{aligned}
\mathcal{B}(B^+ \rightarrow K^+\pi^0) &= (1.88^{+0.55}_{-0.49} \pm 0.23) \times 10^{-5} \\
\mathcal{B}(B^+ \rightarrow \pi^+\pi^0) &= (0.33^{+0.35}_{-0.27} \pm 0.07) \times 10^{-5} \\
\mathcal{B}(B^0 \rightarrow K^0\pi^0) &= (2.10^{+0.93+0.25}_{-0.78-0.23}) \times 10^{-5}
\end{aligned}$$

Since the $\pi^+\pi^0$ result is not statistically significant, we establish the upper limit at 90% CL. by integrating the likelihood to the point that covers 90% of the physically allowed area. We arrive at an upper limit of $\mathcal{B}(B^+ \rightarrow \pi^+\pi^0) < 1.01 \times 10^{-5}$.

IV. CONCLUSIONS

We have measured branching fractions of charmless B decays with $h\pi^0$ in the final states. Our preliminary results are consistent with the published results from the CLEO Collaboration [13]. With more than 10 fb^{-1} data expected to be collected by the end of this year, we expect to determine the $B^+ \rightarrow \pi^+\pi^0$ branching ratio. In the near future, the clear experimental signatures

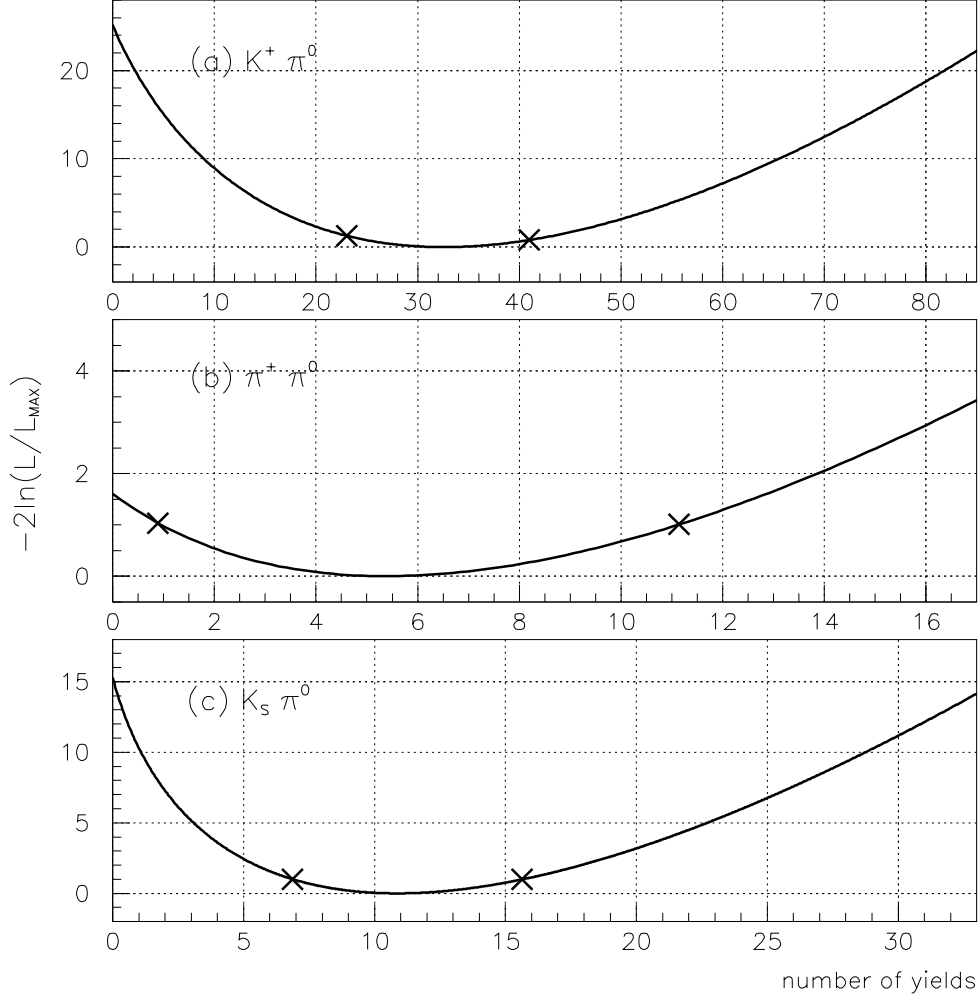


FIG. 2. $-2 \ln(\mathcal{L}/\mathcal{L}_{\max})$ as a function of the number of signal yields for (a) $K^+ \pi^0$, (b) $\pi^+ \pi^0$, and (c) $K_s \pi^0$

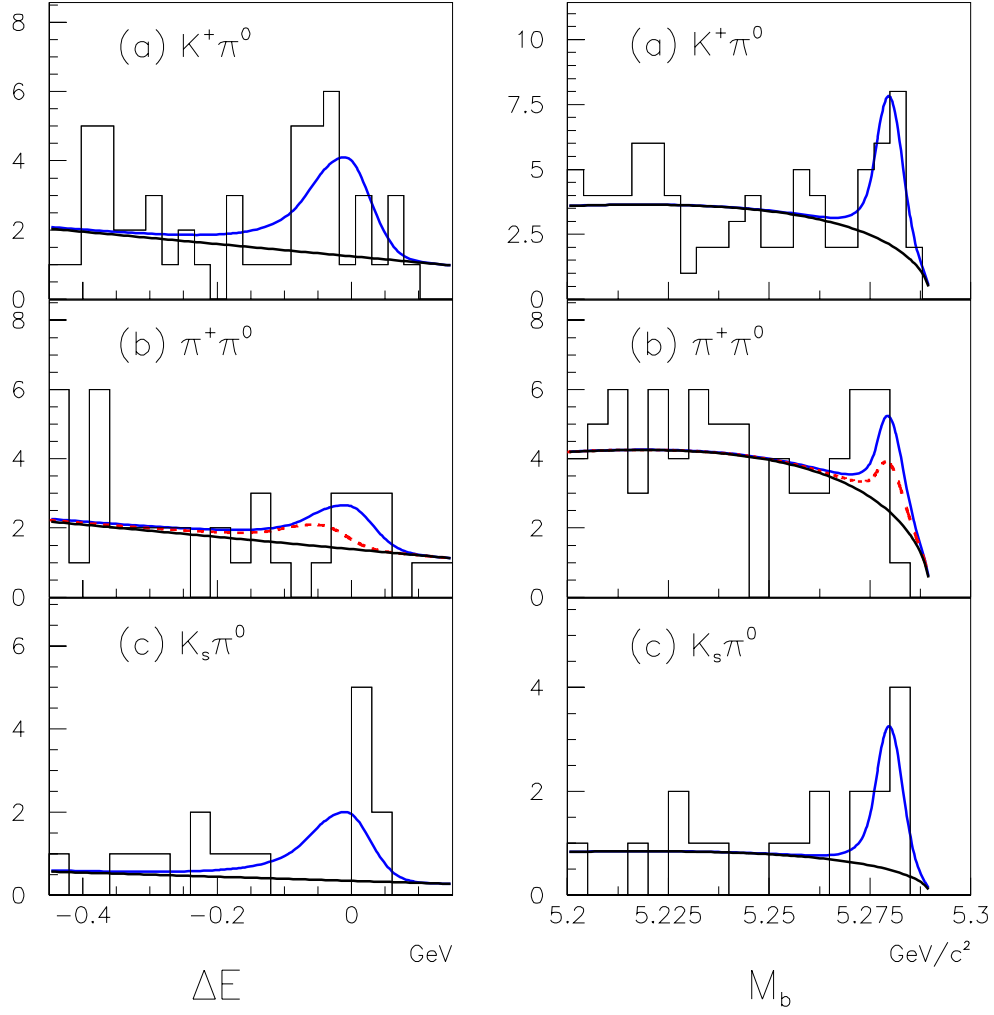


FIG. 3. The projections of the likelihood fits on ΔE and M_b distributions for the (a) $K^+\pi^0$, (b) $\pi^+\pi^0$, and (c) $K_s\pi^0$ cases. Histograms correspond to real data. Dashed lines in (b) indicate the $K^+\pi^0$ feed down expectation.

of $B^+ \rightarrow K^+ \pi^0$ and $\pi^+ \pi^0$ will be used in the search for direct CP violations and the determination of the phase angles ϕ_2 and ϕ_3 .

The $B^+ \rightarrow K_S \pi^0$ mode is of particular interest, since the central value of our measurement is more than a factor of three larger than theoretical expectations. If this high value persists with higher precision, it may indicate the importance of strong final state interaction (FSI) in rare B decays [14].

V. ACKNOWLEDGEMENT

We gratefully acknowledge the efforts of the KEKB group in providing us with excellent luminosity and running conditions and the help with our computing and network systems provided by members of the KEK computing research center. We thank the staffs of KEK and collaborating institutions for their contributions to this work, and acknowledge support from the Ministry of Education, Science, Sports and Culture of Japan and the Japan Society for the Promotion of Science; the Australian Research Council and the Australian Department of Industry, Science and Resources; the Department of Science and Technology of India; the BK21 program of the Ministry of Education of Korea and the Basic Science program of the Korea Science and Engineering Foundation; the Polish State Committee for Scientific Research under contract No.2P03B 17017; the Ministry of Science and Technology of Russian Federation; the National Science Council and the Ministry of Education of Taiwan; the Japan-Taiwan Cooperative Program of the Interchange Association; and the U.S. Department of Energy.

REFERENCES

- [1] N. Cabibbo, *Phys. Rev. Lett.* **10**, 531, (1964).
M. Kobayashi and T. Maskawa, *Prog. Th. Phys.* **49**, 652 (1973).
- [2] R. Fleischer, *Int.J.Mod.Phys.* **A12**, 2459 (1997).
- [3] H. J. Lipkin *et al.*, *Phys. Rev. D* **44**, 1454 (1991).
Y. Nir and H. R. Quinn, *Phys. Rev. Lett.* **67**, 541 (1991).
- [4] M. Gronau and J. L. Rosner and D. London, *Phys. Rev. Lett.* **73**, 21 (1994);
O. F. Hernández, *et al.*, *Phys. Lett. B* **333**, 500 (1994);
M. Gronau *et al.*, *Phys. Rev. D* **50**, 4529 (1994).
- [5] BELLE Collaboration, Technical Design Report, KEK Report 95-1, 1995.
- [6] KEKB accelerator group, KEKB B Factor Design Report, KEK Report 95-7, 1995;
K. Akai *et al.*, "COMMISSIONING OF THE KEKB B-FACTORY", WEAR4, Proc. 1999 Particle Accelerator Conference, New York (1999);
F. Funakoshi *et al.*, "KEKB PERFORMANCE", Proc. 2000 European Particle Accelerator-Conderence, Vienna (2000).
- [7] G. Alimonti *et al.*, KEK preprint 2000-34.
- [8] H. Hirano *et al.*, KEK Preprint 2000-2, submitted to Nucl. Inst. Meth.; M. Akatsu *et al.*, DPNU-00-06, submitted to Nucl. Inst. Meth.
- [9] T. Iijima *et al.*, Proceedings of the 7th International Conference on Instrumentation for Colliding Beam Physics, Hamamatsu, Japan, Nov 15-19, 1999.
- [10] H. Kichimi *et al.*, submitted to Nucl. Inst. Meth.
- [11] H. Ikeda *et al.*, Nucl. Inst. Meth. **441**, 401 (2000).
- [12] G. Fox and S. Wolfram, *Phys. Rev. Lett.* **41**, 1581 (1978).
- [13] CLEO Collaboration, D. Cronin-Hennessy *et al.*, CLNS 99/1650, CLEO 99-18, Submitted to Phys. Rev. Lett.
J. Smith, "Status of Charmless Hadronic B Decays with the Full CLEO Data Sample", will be published in the proceedings of the Third International Conference on B Physics and CP Violation, Taipei, Taiwan, December 3-7, 1999
- [14] W. Hou and K. Yang, *Phys. Rev. Lett.* **84**, 4806 (2000).